PHYSICAL REVIEW B **93**, 041423(R) (2016)

Polarization coupling transition in $BaTiO_3/PbZr_{0.2}Ti_{0.8}O_3$ ferroelectric bilayers

Pavel Salev, Abdulah Mahayni, and Alexei Grigoriev*
The University of Tulsa, Tulsa, Oklahoma 74104, USA
(Received 14 December 2015; published 29 January 2016)

Electrostatic interactions between thin films of two different ferroelectric materials lead to a layer of free charges localized at the interface between ferroelectrics according to a computational analysis presented in this work. The free charges at the interface between $BaTiO_3$ and $PbZr_{0.2}Ti_{0.8}O_3$ reduce polarization coupling strength significantly. This helps the layers to retain most of their single-layer polarizations and enables a layer-by-layer polarization switching, which has been observed in recent experimental studies. The sheet carrier density at the interface decreases by at least eight orders of magnitude when the film thickness is reduced from 30 to 10 nm. This drop in the carrier density is accompanied by a strong increase of polarization coupling between ferroelectric layers. This polarization coupling transition can explain the difference between strong coupling in thin ferroelectric superlattices and weak coupling in thicker multilayer films.

DOI: 10.1103/PhysRevB.93.041423

I. INTRODUCTION

Ferroelectric multilayers and superlattices provide a pathway to engineer novel materials with enhanced functional properties in respect to the properties of single-layer materials [1–6]. Utilizing several oxide materials with different ferroelectric properties and crystal lattice parameters to build a multilayer system can be beneficial for design of complex internal electric fields and epitaxial strain profiles, which control ferroelectric and dielectric properties of a new heterostructure [7]. Most studies of ferroelectric heterostructures were focused on ferroelectric-paraelectric systems. All-ferroelectric multilayer materials, however, provide even more flexibility for tailoring the polarization profile inside the layers providing great opportunities for enhancing and introducing properties that cannot be found in other systems. Examples of new functional properties in all-ferroelectric multidomain and multilayer systems include switchable domain wall conductivity in $BaTiO_3$ and $BiFeO_3$ ferroelectrics [8–10], and layer-by-layer polarization switching in a $BaTiO_3/PbZr_{0.2}Ti_{0.8}O_3$ (BTO/PZT) bilayer that results in double polarization hysteresis [11]. The layer-by-layer switching enables tail-to-tail and head-to-head polarization domain configurations, which have distinct ferroelectric and dielectric properties, multiplying the number of possible switchable states in this system.

Polarization gradient and concomitant depolarizing fields in antiparallel ferroelectric domains or layers of different ferroelectric materials can be compensated, at least partially, by an increase of free-charge carrier density at the interfaces. The free interface charges are predicted to occupy the interface space-charge region as a result of semiconductor band bending of oxide layers under strong internal depolarizing fields [10,12]. These predictions have been made considering ferroelectric oxides as wide-band-gap semiconductor materials [10,12–14]. The width of the interfacial space-charge region and, consequently, the polarization coupling strength depend on a delicate balance between depolarizing fields and the free-charge carrier distribution near the interface [10,12,15,16]. This balance should be a function of a ferroelectric layer thickness considering that the polarization coupling strength may be different in thick- and thin-layer films because the thickness of the layers can become comparable to the space-charge region width in thinner-layer heterostructures. In thicker multilayer films, the coupling can become weak assuming the free charges at the interface provide sufficient compensation to screen the internal electric fields and maintain a large polarization gradient between the layers. The goal of our computational study is to investigate the thickness dependence of polarization coupling strength in $BaTiO_3/PbZr_{0.2}Ti_{0.8}O_3$ ferroelectric bilayer in order to better understand the coupling phenomena in ferroelectric multilayers and to guide design of multilayer materials with desirable properties.

II. METHODS

The modeling of a ferroelectric system that includes space-charge regions can be undertaken using a combination of thermodynamic Landau-Ginzburg-Devonshire (LGD) and semiconductor theories [10]. A one-dimensional model of a ferroelectric material can be described by the two differential equations that couple the electric polarization P and the electrostatic potential φ [17–19]:

$$-\varepsilon_b\varepsilon_0\frac{d^2\varphi}{dx^2}+\frac{dP}{dx}=\rho(\varphi)\,, \tag{1}$$

$$\alpha P+\beta P^3+\gamma P^5-g\frac{d^2P}{dx^2}+\frac{d\varphi}{dx}=0, \tag{2}$$

where ε_b and ε_0 are background and free-space permittivities, respectively; and $\alpha,\ \beta,\ \gamma$, and g are free-energy expansion coefficients. The first equation represents the Gauss law, and the second equation is a result of minimization of the LGD free-energy expansion. The free-energy expansion coefficients can be renormalized to include the effects of epitaxial strain [20]. The free-charge density depends on the electrostatic potential φ as [21]

$$\rho(\varphi)=-qN_cF_{1/2}\left(\frac{E_F-E_c+q\varphi}{k_BT}\right)+qN_vF_{1/2}\left(\frac{E_v-E_F-q\varphi}{k_BT}\right), \tag{3}$$

*alexei-grigoriev@utulsa.edu

 ©2016 American Physical Society

where q is the elementary charge; N_c and N_v are the densities of states in conduction and valence bands, respectively; k_B is the Boltzmann constant; T is temperature; and $F_{1/2}$ is the Fermi-Dirac integral. E_c and E_v are the energies of the bottom of the conduction band and the top of the valence band, respectively, and E_F is the Fermi energy. These energies are defined in respect to the vacuum level. The system of equations (1) and (2) for the BTO/PZT bilayer can be solved numerically using mixed boundary conditions:

$$\varphi(-h) = 0, \quad \varphi(+h) = \Delta W, \quad \frac{dP}{dx}(x = \pm h) = 0, \tag{4}$$

where h is the thickness of ferroelectric layers, and ΔW is the work function difference between BTO and PZT. In this work we used the same thickness h for both BTO and PZT layers. The requirement that the derivative of polarization is a zero at the ends of the bilayer corresponds to ideal screening of polarization by free charges of electrodes [22]. Semiconductor structure parameters and LDG free-energy coefficients for BTO and PZT were obtained from the literature [10,23–25]. The coupled differential equations (1) and (2) were solved using COMSOL software.

III. RESULTS

Band structure, free-charge carrier concentration, polarization, and electric field distributions, that were obtained by solving Eqs. (1) and (2), are shown in Fig. 1 for 300-nm (solid lines) and 30-nm (dashed lines) BTO/PZT relaxed bilayers. The results are presented on the length scale that is normalized by the layer thickness. For these calculations, the BTO polarization pointed toward the bilayer interface and the PZT polarization pointed away from it. The electric fields introduced by the polarization gradient bend the electronic energy bands strongly enough for the top of the valence band to cross the Fermi level. This band bending leads to a sharp increase of the concentration of free-charge carriers near the BTO/PZT interface. The charge carriers are holes for the chosen polarization configuration, but they will change to electrons if polarization direction is reversed at the interface. The relative width of the space-charge region is noticeably larger in the thinner bilayer. Free charges in the interfacial space-charge region reduce depolarizing fields, which enables large polarization gradients between the layers as a stable configuration of the system. As expected, the screening effect of the interfacial free charges is weaker in thinner films, which leads to stronger depolarizing fields and a smaller stable polarization gradient in thinner layers than in thicker ones.

The effectiveness of depolarizing field screening may decrease dramatically when the layers get thinner than the space-charge region width. The electric polarization in the middle of BTO and PZT layers and other polarization coupling related properties are shown in Fig. 2 as a function of ferroelectric layer thickness from 3 to 500 nm. These calculations were done at each thickness for fully relaxed layers and for the layers that were completely strained as if they were grown on $SrTiO_3$ (100) substrate that has a 3.905-Å in-plane lattice constant [26–28]. Including strain in calculations is important because the epitaxial strain can modify significantly ferroelectric properties of thin films [29,30]. The BTO and

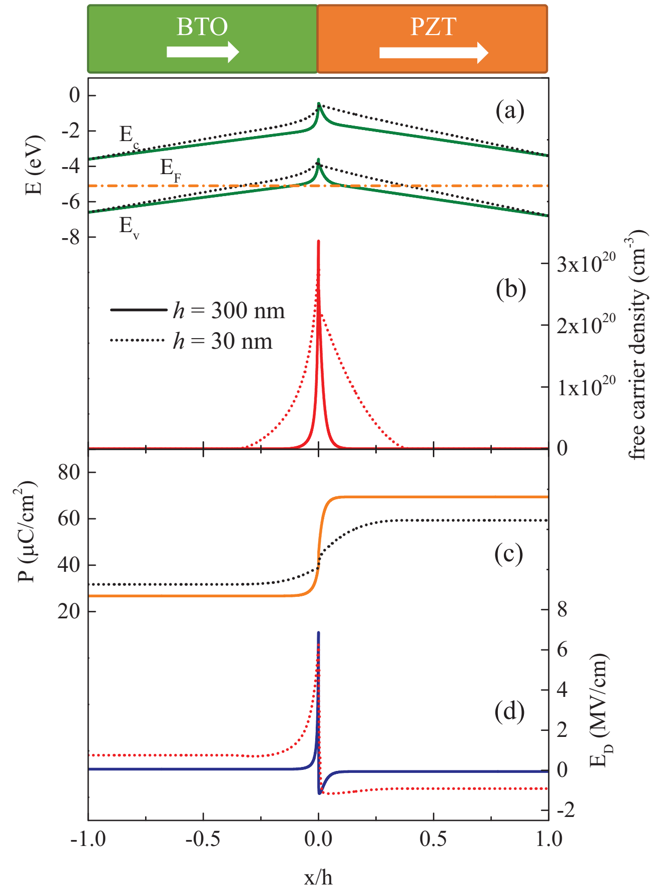

FIG. 1. (a) Electron energy band diagram, (b) free carrier density, (c) electric polarization, and (d) depolarizing field as a function of x/h normalized position across the $BaTiO_3/PbZr_{0.2}Ti_{0.8}O_3$ bilayer model (shown schematically on the top).

PZT layers in the bilayer system retain almost completely the magnitudes of single-layer electric polarizations if these layers are thicker than 70 nm [Fig. 2(a)]. In thinner bilayers, the electric polarizations change dramatically, and the BTO-layer polarization becomes almost the same as the polarization of PZT in layers thinner than 15 nm for relaxed and 9 nm for fully strained films. Depolarizing fields in ferroelectric layers increase monotonically with decreasing the film thickness until the fields become almost insensitive to film thickness changes in thinner films [Fig. 2(b)]. Interestingly, we found that the monotonic increase of the depolarizing fields in thicker bilayers is well described by a simple estimate of the field due to charged domain walls of a single-layer ferroelectric material [10]: $E_D \cong E_{gap}/(qh)$, where E_{gap} is the band gap of ferroelectric.

The free-charge carrier density increases sharply near the BTO/PZT interface resembling a two-dimensional gas of electrons or holes depending on polarization configuration. The properties of this two-dimensional gas can be quantified as the sheet carrier density:

$$n = \frac{1}{q}\int_{-h}^{+h} \rho(x)dx. \tag{5}$$

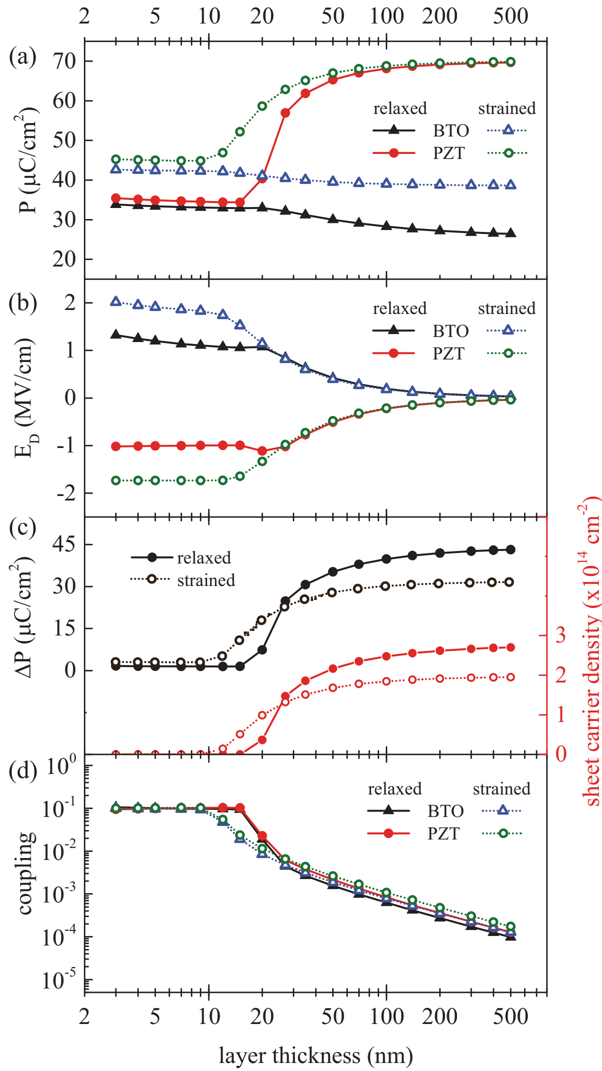

FIG. 2. (a) Electric polarizations, (b) depolarizing fields, (c) polarization differences and sheet carrier densities, and (d) polarization coupling strengths as a function of the thickness of BTO and PZT ferroelectric layers for relaxed and strained bilayer models.

This density follows the changes of the BTO/PZT polarization difference [Fig. 2(c)] indicating a positive correlation between polarization gradient and conductivity of the interface boundary. The sheet carrier density decreases by 8 to 24 orders of magnitude when the layer thickness decreases from 30 to 15 nm for relaxed and to 9 nm for strained layers. The thickness at which the carrier density starts to increase quickly can be interpreted as the critical thickness of charged interface formation.

The polarization contrast between BTO and PZT reduces to 1–2 μC/cm^2 when the layers are thinner than the critical thickness. This resembles strong polarization coupling behavior predicted by the nonlinear thermodynamic model (NLTM) developed for ideal insulating ferroelectric multilayers [31]. A polarization coupling coefficient κ can be used in order to quantify coupling [15]:

$$E_D = \frac{\kappa}{2\varepsilon_b\varepsilon_0}\Delta P, \qquad (6)$$

where ΔP is the polarization contrast between BTO and PZT layers. The coupling coefficient was introduced in the NLTM as an independent parameter accounting for unknown free charges in ferroelectric layers. This coefficient can be obtained automatically from results of our calculations using a combination of semiconductor and thermodynamics models [Fig. 2(d)]. The coupling increases from $\kappa \approx 10^{-4} - 10^{-3}$ in thicker films to a weakly changing value of $\kappa \approx 0.1$ below the critical thickness. Such small coupling coefficient in thicker films agrees well with recently reported weak polarization coupling in experimentally studied ferroelectric bilayers [32,33]. The NLTM assumes a steplike change of the electric polarization at the ferroelectric-ferroelectric interface. This assumption allows the coupling coefficient to reach $\kappa_{\max} = 1$. The model that includes semiconductor energy bands will always introduce a transitional space-charge region at the interface between two semiconductors. This will prohibit infinitely sharp steplike polarization jumps at the interface, and the coupling coefficient will never reach the absolute maximum of $\kappa_{\max} = 1$. When the coupling coefficient reaches its maximum $\kappa \approx 0.1$ in a thin BTO/PZT bilayer, the depolarizing field in PZT gets close to the theoretical switching field predicted for PZT material by the Landau-Devonshire thermodynamic theory. Since the depolarizing field in PZT layer opposes the electric polarization, one can expect antiparallel polarization domains to form in PZT to reduce the electrostatic potential energy [34].

The ferroelectric-paraelectric phase transition temperature depends on epitaxial strain and internal electric field. The effect of the depolarizing field on temperature of ferroelectric phase transitions in the layers of BTO/PZT bilayer was analyzed for 500-, 100-, and 20-nm relaxed layers (Fig. 3). Even in the thickest modeled bilayer the BTO layer retains a noticeable polarization up to the PZT transition temperature of 681 K that is just slightly lower than the phase transition temperature of pure PZT. The depolarizing field of 35–40 kV/cm does not change much at temperatures below the transition temperature. As the coupling gets stronger in thinner films, the electric fields inside the layers increase to 200–220 kV/cm in a 100-nm bilayer up to the transition temperature of 633 K, at which both PZT and BTO layers lose their polarization quickly. The BTO layer maintains a relatively large polarization of about 12 μC/cm^2 until the transition at 633 K. In a 20-nm bilayer, which is just slightly thicker than the thickness of the room-temperature polarization coupling transition, BTO and PZT layers have almost identical polarizations at temperatures above 400 K. The depolarizing field in this thin bilayer decreases nearly linearly with increasing temperature until 582 K. At this temperature the polarizations of the layers decrease sharply to less than 5 μC/cm^2, but the polarizations and internal electric fields do not vanish completely even at temperatures above the phase transition temperature of pure PZT. This nonvanishing high-temperature polarization can be due to a polarizing effect of built-in field $E_{bi} \sim \Delta W/h$ as a result of the contact potential difference, which continues to affect the thin bilayer even in its paraelectric state.

Ferroelectric layers of the BTO/PZT bilayer system can be considered as capacitors in series because of weak coupling and large interface free-charge density [35]. Using the calculated magnitudes of the internal electric field and polarization

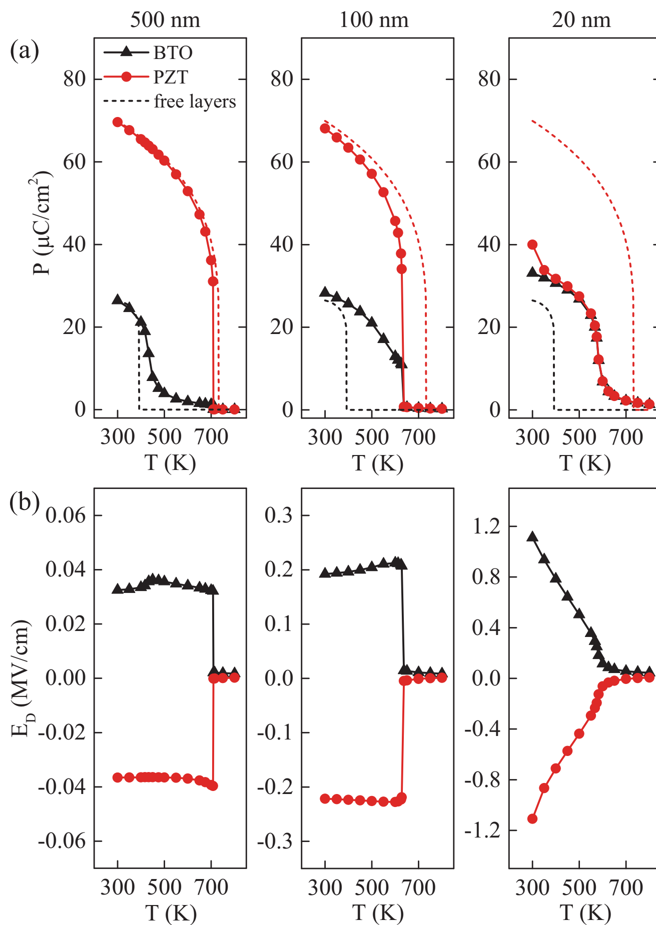

FIG. 3. Temperature dependences of (a) electric polarizations and (b) depolarizing fields inside ferroelectric layers of the BTO/PZT bilayer system. Free-layer polarizations are shown as dashed lines to illustrate the ferroelectric phase transitions in free-standing layers.

in the middle of ferroelectric layers, we could obtain, as a coarse estimate, the relative dielectric permittivities of 149, 129, and 103 for 500-, 100-, and 20-nm bilayers, respectively. These permittivities are larger than the permittivities of single-layer epitaxial PZT films in the tetragonal phase [36]. Considering that a large spontaneous polarization is predicted in the BTO layer at temperatures well above the transition temperature of pure BTO, the permittivity enhancement in respect to the permittivity of a single-layer PZT is likely to persist in the bilayer over a broader temperature range beyond the ferroelectric transition of BTO [37,38]. These findings suggest a possibility to enhance dielectric properties of ferroelectric materials by combining BTO and PZT layers.

IV. CONCLUSIONS

The LGD thermodynamic model in combination with semiconductor theory provides a useful computational approach to analyzing properties of coupled ferroelectric layers and predicting properties of new multilayer materials based on known thermodynamic and electronic structure parameters of system constituents. The results of this approach applied to the BTO/PZT bilayer suggest a sharp polarization coupling transition in films thinner than 20 nm, which is accompanied by dramatic changes of the free-charge carrier density at the interface. These free charges screen the depolarizing fields and enable stable configurations of ferroelectric layers retaining a large polarization contrast. The results support our recent experimental findings of double polarization switching in 120-nm BTO/120-nm PZT ferroelectric bilayers suggesting the electrostatic coupling is so weak that the layer-by-layer polarization switching is possible [11]. The recipe we used for polarization coupling analysis for BTO/PZT bilayer can be applied readily to other wide-band-gap semiconductor ferroelectric heterostructures provided the LGD expansion coefficients and band structure parameters are known. Novel ferroelectric multilayer materials for tunable dielectric devices and other applications can be designed with specific polarization coupling properties, dielectric permittivities, and internal fields using the predictions and approach presented in this Rapid Communication.

ACKNOWLEDGMENT

This work was supported by the National Science Foundation CAREER Award No. DMR-1057159.

[1] M. W. Cole, E. Ngo, S. Hirsch, J. D. Demaree, S. Zhong, and S. P. Alpay, J. Appl. Phys. **102**, 034104 (2007).
[2] M. W. Cole, C. V. Weiss, E. Ngo, S. Hirsch, L. A. Coryell, and S. P. Alpay, Appl. Phys. Lett. **92**, 182906 (2008).
[3] M. W. Cole, E. Ngo, C. Hubbard, S. G. Hirsch, M. Ivill, W. L. Sarney, J. Zhang, and S. P. Alpay, J. Appl. Phys. **114**, 164107 (2013).
[4] H. N. Lee, H. M. Christen, M. F. Chisholm, C. M. Rouleau, and D. H. Lowndes, Nature **433**, 395 (2005).
[5] S. S. A. Seo, J. H. Lee, H. N. Lee, M. F. Chisholm, W. S. Choi, D. J. Kim, J. Y. Jo, H. Kim, J. Yu, and T. W. Noh, Adv. Mater. **19**, 2460 (2007).
[6] L. Hong, P. Wu, Y. Li, V. Gopalan, C.-B. Eom, D. G. Schlom, and L.-Q. Chen, Phys. Rev. B **90**, 174111 (2014).
[7] D. Matthew and E. Bousquet, MRS Bull. **38**, 1048 (2013).
[8] A. Bhatnagar, A. Roy Chaudhuri, Y. Heon Kim, D. Hesse, and M. Alexe, Nat. Commun. **4**, 2835 (2013).
[9] L. Feng, S. Yang, Y. Lin, D. Zhang, W. Huang, W. Zhao, Y. Yin, S. Dong, and X. Li, Appl. Mater. Interfaces **7**, 26036 (2015).
[10] T. Sluka, A. K. Tagantsev, D. Damjanovic, M. Gureev, and N. Setter, Nat. Commun. **3**, 748 (2012).
[11] P. Salev and A. Grigoriev (unpublished).
[12] Y. Xiao, V. B. Shenoy, and K. Bhattacharya, Phys. Rev. Lett. **95**, 247603 (2005).
[13] L. Pintilie, M. Lisca, and M. Alexe, Integr. Ferroelectr. **73**, 37 (2005).
[14] J. F. Scott, *Ferroelectric Memories* (Springer Science & Business Media, Berlin, 2000), Vol. 3.
[15] M. B. Okatan, J. V. Mantese, and S. P. Alpay, Phys. Rev. B **79**, 174113 (2009).

[16] Y. Y. Liu and J. Y. Li, Appl. Phys. Lett. **97**, 042905 (2010).
[17] J. Muller, T. S. Boscke, U. Schroder, S. Mueller, D. Brauhaus, U. Bottger, L. Frey, and T. Mikolajick, Nano Lett. **12**, 4318 (2012).
[18] M. Y. Gureev, A. K. Tagantsev, and N. Setter, Phys. Rev. B **83**, 184104 (2011).
[19] E. A. Eliseev, A. N. Morozovska, G. S. Svechnikov, V. Gopalan, and V. Y. Shur, Phys. Rev. B **83**, 235313 (2011).
[20] N. A. Pertsev, A. G. Zembilgotov, and A. K. Tagantsev, Phys. Rev. Lett. **80**, 1988 (1998).
[21] S. M. Sze and K. K. Ng, *Physics of Semiconductor Devices* (John Wiley & Sons, New York, 2006).
[22] I. B. Misirlioglu, G. Akcay, S. Zhong, and S. P. Alpay, J. Appl. Phys. **101**, 036107 (2007).
[23] K. M. Rabe, C. H. Ahn, and J.-M. Triscone, *Physics of Ferroelectrics: A Modern Perspective* (Springer Science & Business Media, Berlin, 2007), Vol. 105.
[24] J. F. Scott, Jpn. J. Appl. Phys. **38**, 2272 (1999).
[25] B. Völker, C. M. Landis, and M. Kamlah, Smart Mater. Struct. **21**, 035025 (2012).
[26] C. J. Xiao, C. Q. Jin, and X. H. Wang, Mater. Chem. Phys. **111**, 209 (2008).
[27] J. Frantti, J. Lappalainen, S. Eriksson, V. Lantto, S. Nishio, M. Kakihana, S. Ivanov, and H. Rundlöf, Jpn. J. Appl. Phys. **39**, 5697 (2000).
[28] R. H. Mitchell, A. R. Chakhmouradian, and P. M. Woodward, Phys. Chem. Miner. **27**, 583 (2000).
[29] D. G. Schlom, L.-Q. Chen, C. J. Fennie, V. Gopalan, D. A. Muller, X. Pan, R. Ramesh, and R. Uecker, MRS Bull. **39**, 118 (2014).
[30] J. S. Speck, A. Seifert, W. Pompe, and R. Ramesh, J. Appl. Phys. **76**, 477 (1994).
[31] A. L. Roytburd, S. Zhong, and S. P. Alpay, Appl. Phys. Lett. **87**, 092902 (2005).
[32] P. Salev, M. Meisami-Azad, and A. Grigoriev, J. Appl. Phys. **113**, 074104 (2013).
[33] A. Grigoriev, C. Yang, M. Meisami Azad, O. Causey, D. A. Walko, D. S. Tinberg, and S. Trolier-McKinstry, Phys. Rev. B **91**, 104106 (2015).
[34] F. A. Urtiev, V. G. Kukhar, and N. A. Pertsev, Appl. Phys. Lett. **90**, 252910 (2007).
[35] F. C. Sun, M. T. Kesim, Y. Espinal, and S. P. Alpay, J. Mater. Sci. **51**, 499 (2015).
[36] I. Vrejoiu, G. L. Rhun, L. Pintilie, D. Hesse, M. Alexe, and U. Gösele, Adv. Mater. **18**, 1657 (2006).
[37] J. Zhang, A. A. Heitmann, S. P. Alpay, and G. A. Rossetti, Jr., J. Mater. Sci. **44**, 5263 (2009).
[38] Q. Y. Qiu, R. Mahjoub, S. P. Alpay, and V. Nagarajan, Acta Mater. **58**, 823 (2010).